Hygro-mechanical modeling of cracked concrete in the framework of the X-FEM

S. Jox, C. Becker & G. Meschke
Institute for Structural Mechanics, Ruhr-University Bochum, Germany

ABSTRACT: Consideration of moisture transport in addition to external loading is a prerequistite for reliable durability analyses of structures made of concrete. The presentation is concerned with the modeling of cohesive cracks in partially saturated cementitious materials using the Extended Finite Element Method (X-FEM), focussing on the interactions between cracks and moisture transport. To this end, a coupled hygro-mechanical model for partially saturated concrete is extended for the consideration of cracks in the context of a 3D X-FEM model. Moisture flow within crack planes is accounted for by assuming Poiseuille flow within the crack planes, taking the tortuousity and the crack width dependence of the liquid permeability within cracks into account. For the three-dimensional implementation of the X-FEM formulation a higher-order spatial discretization concept based on Legendre polynomials is used. The applicability of the hygro-mechanical X-FEM-model is investigated by means of a representative 3D benchmark example considering a hygro-mechanical loading scenario.

1 INTRODUCTION

Numerical prognoses of durability of structures made of cementitious materials such as concrete or geomechanical analyses require the consideration of moisture transport together with and the hygro-mechanical couplings governing the hygro-mechanial response of porous materials (see, e.g. (Coussy 2004; Lewis and Schrefler 1998)). In particular, transport of moisture within opening and evolving discontinuities such as cracks in concrete and shear bands in soils has to be taken into account in these analyses. For reliable durability analyses of cementitious materials such as concrete (Coussy and Ulm 2001), the highly accelerated moisture transport in cracks is a major source for corrosive processes.

The paper is concerned with a concept for coupled hygro-mechanical analyses of partial saturated cementititous materials in the in the framework of the BIOT-COUSSY theory considering discontinuities of the displacement field representing the opening of cracks taking the influence of discrete cracks on the liquid permeability of concrete into account (Barton, Bandis, and Bakhtar 1985; Meschke and Grasberger 2003). To this end, the Extended Finite Element Method (X-FEM) (Moës, Dolbow, and Belytschko 1999; Abellan, de Borst, and Bergheau 2005) is employed for the discrete representation of cracks in concrete structures.

The numerical representation of continuous crack paths, as it is required in X-FEM-analyses, in three dimensions is a difficult and challenging task. However, a few fully three-dimensional applications of the X-FEM to crack propagation analyses have been published in the recent years (Sukumar, Moës, Moran, and Belytschko 2000; Sukumar, Chopp, and Moran 2003; Gasser and Holzapfel 2005). In several cases the crack topology and the propagation of cracks has been described implicitly (Moës, Gravouil, and Belytschko 2002; Gravouil, Moës, and Belytschko 2002) by the *level-set-method* (Osher and Fedkiw 2003).

For the spatial discretization in structural mechanics, the p-version of the finite element method has proven to be an efficient and powerful tool (Düster 2002; Szabó, Düster, and Rank 2004), in particular due to its ability to avoid locking effects that occur when a non-adequate element kinematics is used. The field of application of the p-finite element method has been extended during the last decade. Besides linear analyses, also geometrically nonlinear (Ander and Samuelsson 2001) as well as materially nonlinear (Düster and Rank 2002) problems were solved adequately. Also for multi-physics problems like thermo-mechanically (Düster, Niggl, and Rank 2002) or chemo-mechanically coupled problems (Kuhl, Bangert, and Meschke 2004) the p-version has been successfully applied. The p-FEM as well as the X-FEM allow for the use of meshes that consist of relatively large elements. In the X-

FEM, the crack can be introduced discretely without mesh adaption or mesh refinement. The proposed approach aims at a combination of both methods to benefit from their properties when simulating hygro-mechanical problems in concrete structures.

The paper is organized as follows: A concise summary of the kinematics considering discontinuities and the model for partially saturated cementitious materials ion in the context of hygro-mechanical coupled problems is presented in Sections 2 and 3. Section 4 is concerned with a model for moisture transport in cracked materials considering tortuousity effects in a phenomenological manner. The use of the spatial p finite element method is described in Section 5. The finite element formulation of the X-FEM model enhanced for partial saturated cracked structures is described in Section 6, considering enrichment functions for open cracks. The benchmark example described in Section 7 investigates the applicability of the model using an anisotropic 3D-p-element in the context of a hygro-mechanical analysis of a concrete beam.

2 KINEMATICS: DISCONTINOUS DISPLACEMENT FIELD

A domain Ω of a body $\mathcal{B}$ is considered to be separated into two parts Ω^+ and Ω^- by means of a localization surface $\partial_S\Omega$ which is defined by the local coordinate system with its normal vector $\mathbf{n}_S$ and its tangential vector $\mathbf{t}_S$ (Figure 1). The displacement field $\mathbf{u}$ is additively decomposed into a continuous part $\bar{\mathbf{u}}$ and a discontinuous part $\check{\mathbf{u}}$ as follows

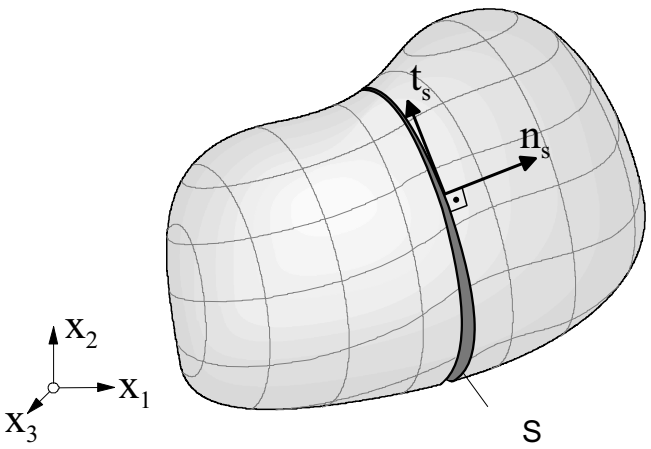

Figure 1: Body $\mathcal{B}$ separated into two parts Ω^+ and Ω^- by localization surface $\partial_S\Omega$

$$\mathbf{u}(\mathbf{x}) \;=\; \bar{\mathbf{u}}(\mathbf{x}) \;+\; \check{\mathbf{u}}(\mathbf{x}), \quad \forall \mathbf{x} \in \Omega, \tag{1}$$

with $\check{\mathbf{u}}(\mathbf{x}) \;=\; S_S(\mathbf{x})\,\hat{\mathbf{u}}(\mathbf{x})$ where $\bar{\mathbf{u}}$ and $\hat{\mathbf{u}}$ are continuous functions in Ω and $S_S(\mathbf{x})$ is the SIGNUM-function defined as

$$S_S(\mathbf{x}) \;=\; \begin{cases} 1 & \forall \mathbf{x} \;\in\; \Omega^+ \\ -1 & \forall \mathbf{x} \;\in\; \Omega^-. \end{cases} \tag{2}$$

The amplitude of the displacement field at the discontinuity $\partial_S\Omega$ is given as

$$[\![\mathbf{u}]\!] \;\; = 2\,\hat{\mathbf{u}} \quad \forall \quad \mathbf{x} \in \partial_S\Omega. \tag{3}$$

The geometrically linear strain field $\boldsymbol{\varepsilon}$ is obtained by taking the (symmetric) gradient according to the equation (1)

$$\boldsymbol{\varepsilon}(\mathbf{u}) \;=\; \underbrace{\nabla^S\bar{\mathbf{u}} \;+\; S_S\nabla^S\hat{\mathbf{u}}}_{\text{regular}} \;+\; \underbrace{2\,(\hat{\mathbf{u}} \otimes \mathbf{n}_S)^S\,\delta_S}_{\text{singular}}. \tag{4}$$

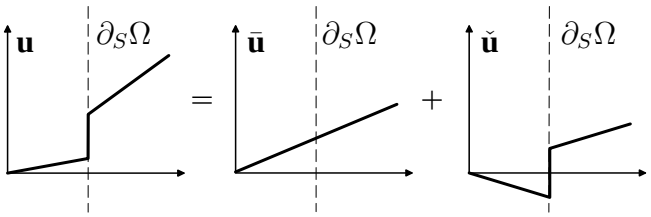

Figure 2: Decomposition of the displacement field

3 HYGRO-MECHANICAL MODEL FOR PARTIALLY SATURATED CONCRETE

The extension to a coupled hygro-mechanical model is formulated in the framework of the BIOT-COUSSY theory of porous media. Full coupling between moisture transport and the mechanical behaviour of concrete is taken into account. Hence, moisture movement may initiate cracks (e.g., in restrained drying processes), and, in turn, cracks strongly affect the permeability of the material.

We consider the macroscopic capillary-pressure p_c as the driving force for moisture transport

$$p_c \;=\; p_g \;-\; p_l \tag{5}$$

with the gaseous pressure p_g and the liquid pressure p_l. Provided that there is thermodynamically equilibrium between the mixture of water vapour and dry air and the external athmosphere, it may be assumed that the gaseous phase is at constant athmospheric pressure, taken as zero $p_g = 0$ (Bear and Bachmat 1991). Therefore, for the sake of simplicity, the capillary-pressure is expressed as $p_c = -p_l$ in what follows.

In cementitious materials such as concrete, saturation-dependent internal stresses develop as a consequence of molecular adsorption and capillary condensation. When subjected to drying, the internal stresses may lead to severe cracking in concrete structures when the material strength is exhausted, see Figure 3. Structural effects connected with restrained deformations resulting from inhomogenities of the material of the material at the micro- and meso-level and the non-uniform moisture distribution associated with the geometry of the structure must be considered.

The coupling coefficients are identified in this section. The BIOT coefficient b and the BIOT modulus

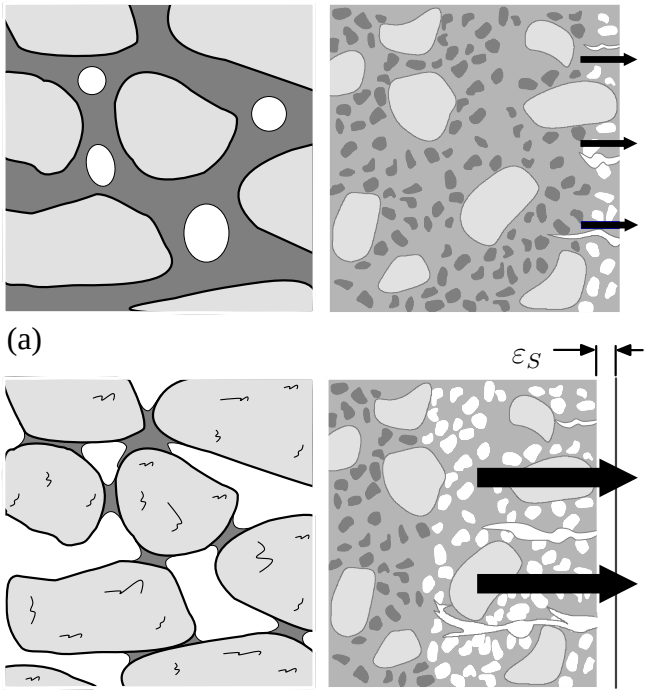

Figure 3: (a) Moisture transport induces capillary-pressure; (b) Cracks promote transport of moisture and aggresive substances

M are obtained as (Grasberger and Meschke 2003; Meschke and Grasberger 2003)

$$b \;=\; S_l \left[1 - \frac{\mathbf{1} : \mathbf{C} : \mathbf{1}}{9\,K_S}\right] \qquad M^{-1} \;=\; \phi_l \frac{\partial S_l}{\partial p_l} \tag{6}$$

see also (Lewis and Schrefler 1998) for a similar formulation. The volumetric marcroscopic stress $\sigma = tr\boldsymbol{\sigma}/3$ is expressed in terms of the solid matrix stress σ' and the liquid pressure p_l as

$$\sigma \;=\; (1-\phi)\sigma' \;-\; \phi_l p_l \tag{7}$$

where ϕ_l is the part of the porosity ϕ filled with liquid water. Based upen the pore network model of (Mualem 1976), the following relation between the capillary pressure and the liquid saturation is proposed in (van Genuchten 1980)

$$S_l(p_c) = \left[1 + (p_c/p_r)^{\frac{1}{1-m}}\right]^{-m} \quad \text{for} \quad p_c \;>\; 0. \tag{8}$$

with the reference pressure $p_r = 18.6237\,N/mm^2$ and the coefficient $m = 0.4396$ specified in (Baroghel-Bouny, Mainguy, Lassabatère, and Coussy 1999).

The total stresses $\boldsymbol{\sigma}$ can be expressed as a function of the effective matrix stresses $\boldsymbol{\sigma}'$, the BIOT coefficient b and the capillary pressure p_c

$$\boldsymbol{\sigma} \;=\; \boldsymbol{\sigma}' \;+\; b p_c \mathbf{1}. \tag{9}$$

4 MOISTURE TRANSPORT MODEL

The moisture transport properties of concrete are strongly affected by changes of the microstructure (Jox, Dumstorff, and Meschke 2006). Flow of moisture within porous materials is assumed to be described by a diffusion model providing a (in general nonlinear) relation between the moisture flux $\mathbf{q}_l$ and the spatial gradient of the liquid pressure ∇p:

$$\mathbf{q}_l \;=\; \frac{\rho_l}{\mu_l}\mathbf{k}_f(S_l)k_\phi(\phi)\,\nabla p_c \tag{10}$$

with the liquid permeability matrix $\mathbf{k}_f$, the dynamic viscosity of liquid μ_l, the porosity ϕ and the mass density ρ_l.

The moisture flux along one single crack is modeled taking the solution of the NAVIER-STOKES equation for plane POISEUILLE flow with an idealized crack formation, assumed to be planar, parallel and of constant opening width w_c, as a starting point:

$$q_l \;=\; \frac{w_c^2}{12\,\mu_l}\nabla p_c. \tag{11}$$

Following the approach of (Barton, Bandis, and Bakhtar 1985) to take into account the roughness of the cracks as well as the aperture variation and tortuousity effects, the mechanical crack width w_c is replaced by

$$w_h \;=\; \frac{w_c^2}{R^{2.5}} \quad \text{for} \quad w_c \geq w_h \tag{12}$$

where $w_c =$ the nominal and $w_h =$ the equivalent hydraulic crack width in μm and the parameter R describes the roughness of the crack. The model parameter R is evaluated by means of a reanalysis of two different series of tests performed by (Aldea, Ghandehari, Shah, and Karr 2000; Oshita and Tanabe 2000) to study the dependency of the liquid permeability of concrete on the cracking process under various boundary conditions. This assumption is confirmed by experimental and numerical data shown in Figure 4. Hence the crack permeability

$$k^t_{c0}(w_h) \;=\; \frac{w_h^2}{12} \tag{13}$$

is expressed considering tortuousity effects along the crack channel Ω_S (Snow 1969; Meschke and Grasberger 2003). The permeability of the uncracked matrix material

$$\mathbf{k}_f(S_l) \;=\; k_r(S_l)\mathbf{k}_0 \tag{14}$$

with the intrinsic permeability $\mathbf{k}_0$ and the relative permeability $k_r(S_l)$ given by an analytical expression suggested by (van Genuchten 1980) for soils as

$$k_r(S_l) \;=\; \sqrt{S_l}\left[1 - (1 - S_l^{1/m})^m\right]^2 \tag{15}$$

for $0 < m < 1$. The permeability of the evolving crack channel

$$k^t_c(S_l, w_h) \;=\; k_{rc}(S_l)k^t_{c0}(w_h) \tag{16}$$

depends on $k_{c0}^t(w_h)$ (equation 13) and the relative crack permeability

$$k_{rc}(S_l) \;=\; 8 \cdot 10^{-6} \exp(11.7 S_l) \tag{17}$$

corresponding to the liquid saturation S_l of the crack channel.

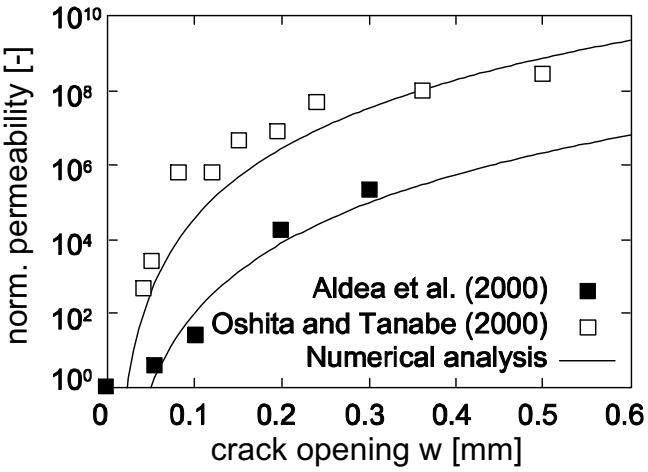

Figure 4: Experimental and numerical data of the relation between crack opening and permeability

5 SPATIAL p-FINITE-ELEMENT-METHOD

The spatial discretization is based on the hierarchically organized LEGENDRE polynomials. The one-dimensional shape functions can be generated by a recursive formula. The shape functions for the three-dimensional brick element are generated by a spatial multiplication of the one-dimensional ones leading to different shape function modes (Becker and Meschke 2004). This allows for spatially anisotropic

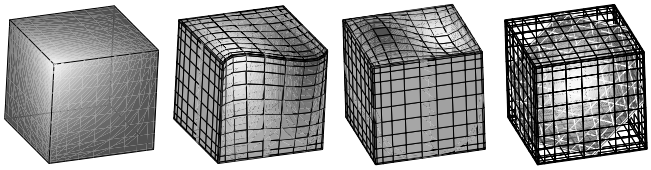

Figure 5: Shape function modes of the p-continuum element: linear nodal mode, p_3-edge mode, $p_{2,3}$-face mode, $p_{2,2,2}$-internal mode

shape functions that can be useful to reduce the computational effort in e.g. shell analyses. In those cases the in-plane degree of approximation of the displacement field can be chosen arbitrarily high, whereas a quadratic or cubic approximation in thickness direction could be sufficient (Becker, Kuhl, and Meschke 2005). Furthermore, because of the hierarchical organisation of the shape functions it is possible to choose the order of approximation in multi-field problems fieldwise. This allows to match the requirements of each field variable without increasing the computational effort by generating totally new shape functions as would be necessary in the LAGRANGEAN discretization concept. In addition, the BABUŠKA-BREZZI-conditions may be fulfilled simply by using TAYLOR-HOOD-like shape functions (Ehlers and Ellsiepen 2001), characterized in hygro-mechanical analyses by the approximation of the displacement field one degree higher than that of the pressure field:

$$p(p_c) = p(\mathbf{u}) - 1. \tag{18}$$

The enhanced displacement field is restricted to a linear approximation to simulate a linear crack opening during crack propagation.

6 ALGORITHMIC FORMULATION AND FINITE ELEMENT IMPLEMENTATION

This section contains details of the finite element formulation of the model. First, the main characteristics and properties of the implementation of the three-dimensional extended finite element method are briefly described, followed by the finite element formulation of the coupled problem.

6.1 *3D X-FEM Implementation*

The basic element is a $3D$-p-brick element that allows for a fieldwise choice of spatially anisotropic shape functions. For the sake of simplicity of the numerical integration and tracing of the crack path in three dimensions, cracks propagate elementwise by intoducing a new plane crack segment into a finite element as soon as crack propagation is being signalled. Therefore, no special crack-tip functions are used but the enhanced degrees of freedom representing the crack opening are set to zero at those facettes of the element that represent the crack-tip. As a crack propagation and crack direction criterion a weighted principal stress criterion is used. Furthermore the implementation includes a traction-separation law with hyperbolic softening to allow for the simulation of cohesive cracks in concrete (Wells and Sluys 2001). The traction-separation law can be turned off to simulate problems linear fracture mechanics-related problems.

To perform the numerical integration at both sides of the crack plane separately, the brick element is subdivided into a fixed set of six tetrahedrons. Depending on how the crack plane is intersecting such a tetrahedron, different subdomains may have to be considered during the numerical integration. For the continuum integration part these subdomains may be pyramids, pentahedra or further tetrahedra. For the integration of the traction-separation law and the moisture flow the subdomains are either triangles or quadrilaterals.

The algorithm to follow the crack path is based on the one presented in (Gasser and Holzapfel 2005).

This algorithm is less strict concerning the C_0-continuity of the crack path compared to other algorithms (see e.g. (Areias and Belytschko 2005)). All element faces or facettes that are cut by a crack will be considered as part of the crack front. Consequently all the elements that are not cut but include the crack front will be considered as potential candidates for "cracked elements".

A crack plane is uniquely defined by a point P in the element and the corresponding normal vector obtained from the principal stress criterion. Figure 6 illustrates how the point P is identified as the vectorial average of all midpoints of the face crack lines. Finally, the crack surface is visualized with the help

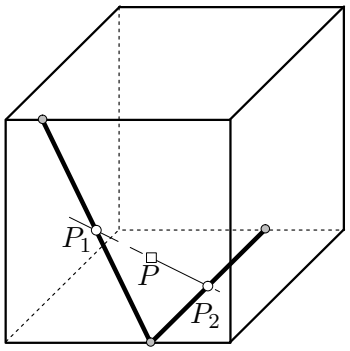

Figure 6: Definition of the base point P of the crack plane within a cracked element

of the level-set $\phi = 0$. Therein ϕ represents the shortest distance of a point and the crack surface and is calculated by the points **P**, **X** and the normal vector $\mathbf{n_S}$:

$$\phi = [\mathbf{X} - \mathbf{P}] \cdot \mathbf{n_S}. \tag{19}$$

6.2 *Hygro-mechanical formulation*

The primary variables within the domain Ω are controlled by the balance of linear momentum and balance of liquid mass:

$$\begin{aligned} &\operatorname{div} \boldsymbol{\sigma} = 0, \\ &\operatorname{div}(\rho_l \mathbf{q}_l) + \dot{m} = 0. \end{aligned} \tag{20}$$

The system of differential equations (20) is completed by the boundery conditions on the boundary Γ given by

$$\boldsymbol{\sigma} \cdot \mathbf{n}_\Gamma = \mathbf{t}^*, \quad \mathbf{q}_l \cdot \mathbf{n}_\Gamma = q_l^*, \quad \mathbf{u} = \mathbf{u}^*, \quad p_c = p_c^* \tag{21}$$

and the initial conditions in the domain Ω given by

$$\mathbf{u}(t=0) = \mathbf{u}_0, \quad p_c(t=0) = p_{c,0}\,, \tag{22}$$

where $\mathbf{n}_\Gamma$ is the normal vector on the boundary surface, q_l^* is the liquid flux across the boundary Γ_q, p_c^* is the prescribed capillary pressure, $\mathbf{u}^*$ is the prescribed displacement and $\mathbf{t}^*$ is the traction vector applied on the boundary Γ_σ.

The weak formulation of the linear balance of momentum together with the respective NEUMANN boundary condition and the weak form of balance of liquid mass together with the respective hygral NEUMANN boundary condition are given as

$$\begin{aligned} \delta W_m &= \int_\Omega \delta\boldsymbol{\varepsilon} : \boldsymbol{\sigma}\, dV - \int_{\Gamma_\sigma} \delta\boldsymbol{u} \cdot \boldsymbol{t}^*\, dA = 0 \\ \delta W_h &= \int_\Omega \delta p_c \frac{\dot{m}_l}{\rho_l}\, dV - \int_\Omega \delta\nabla p_c \cdot \boldsymbol{q}_l\, dV \\ &\quad - \int_{\Gamma_q} \delta p_c\, q_l^*\, dA = 0. \end{aligned} \tag{23}$$

The weak formulation of linear balance of momentum can be written as follows

$$\begin{aligned} \delta W_m^{int} &= \int_\Omega \delta\boldsymbol{\varepsilon} : \boldsymbol{\sigma}\, dV \\ &= \int_\Omega \nabla\delta\bar{\mathbf{u}} : (\boldsymbol{\sigma}' + bp_c\mathbf{1})\, dV \\ &\quad + \int_{\Omega^{+-}} S_S \nabla\delta\hat{\mathbf{u}} : (\boldsymbol{\sigma}' + bp_c\mathbf{1})\, dV \\ &\quad + 2\int_{\partial_S\Omega} \delta\hat{\mathbf{u}} \cdot \underbrace{(\mathbf{t}_S' + bp_c\mathbf{n}_S)}_{\mathbf{t}_S}\, dA \end{aligned} \tag{24}$$

with the total and effective traction vector ($\mathbf{t}_S(\llbracket\mathbf{u}\rrbracket, p_c)$ and $\mathbf{t}_S'(\llbracket\mathbf{u}\rrbracket)$) at the discontinuity surface $\partial_S\Omega$.

Discretization in space yields a coupled set of equations in the standard form (Lewis and Schrefler 1998)

$$\mathbf{S}(\mathbf{x})\dot{\mathbf{x}} + \mathbf{K}(\mathbf{x})\mathbf{x} = \mathbf{r}(\mathbf{x}) \tag{25}$$

with

$$\mathbf{S} = \begin{bmatrix} \mathbf{0} & \mathbf{0} & \mathbf{0} \\ \mathbf{0} & \mathbf{0} & \mathbf{0} \\ \boldsymbol{Q}_{p\bar{u}} & \boldsymbol{Q}_{p\hat{u}} & \boldsymbol{S}_{pp} \end{bmatrix} \tag{26}$$

and

$$\mathbf{K} = \begin{bmatrix} \boldsymbol{K}_{\bar{u}\bar{u}} & \boldsymbol{K}_{\bar{u}\hat{u}} & \boldsymbol{Q}_{\bar{u}p} \\ \boldsymbol{K}_{\hat{u}\bar{u}} & \boldsymbol{K}_{\hat{u}\hat{u}} & \boldsymbol{Q}_{\hat{u}p} \\ \mathbf{0} & \mathbf{0} & \boldsymbol{H}_{pp} \end{bmatrix} \tag{27}$$

and the nodal degrees of freedom and forces

$$\dot{\mathbf{x}} = \begin{bmatrix} \dot{\bar{\boldsymbol{u}}} \\ \dot{\hat{\boldsymbol{u}}} \\ \dot{\boldsymbol{p}} \end{bmatrix} \quad \mathbf{x} = \begin{bmatrix} \bar{\boldsymbol{u}} \\ \hat{\boldsymbol{u}} \\ \boldsymbol{p} \end{bmatrix} \quad \mathbf{r} = \begin{bmatrix} \boldsymbol{r}_{\bar{u}} \\ \boldsymbol{r}_{\hat{u}} \\ \boldsymbol{r}_p \end{bmatrix}. \tag{28}$$

Rewriting equation (25) in a more concise format and applying time discretization using finite differences together with a fully implicit time integration scheme yields a nonlinear system of coupled equations

$$\mathbf{S}(\mathbf{x})\dot{\mathbf{x}} + \mathbf{K}(\mathbf{x})\mathbf{x} = \mathbf{r}(\mathbf{x}) \tag{29}$$

which is solved by means of a NEWTON-RAPHSON procedure after consistent linearization:

$$[\mathbf{S} + \Delta t\,\mathbf{K}]_{n+1}\, \mathbf{x}_{n+1} = \mathbf{S}\,\mathbf{x}_n + \Delta t\,\mathbf{r}_{n+1}. \tag{30}$$

6.3 *Numerical Integration*

For the spatial integration of the stiffness matrix $\mathbf{K}_{\hat{u}\hat{u}}$ and the liquid permeability matrix $\mathbf{H}_{pp}$ different integration domains have to be considered:

$$\begin{aligned}\mathbf{K}_{\hat{u}\hat{u}} &= \int_{\Omega^{+-}} S_S^2\, \mathbf{B}_u^T\, \mathbf{C}\, \mathbf{B}_u\, dV + \int_{\partial_S\Omega} \mathbf{N}_u^T\, \mathbf{T}\, \mathbf{N}_u\, dA \\ \mathbf{H}_{pp} &= -\int_{\Omega} \mathbf{B}_p^T\, \mathbf{k}_f/\mu_l\, \mathbf{B}_p\, dV \\ &\quad - \int_{\Omega_S} \mathbf{B}_p^T\, \mathbf{A}^T\, k_c^t(w)/\mu_l\, \mathbf{A}\, \mathbf{B}_p\, dV.\end{aligned} \tag{31}$$

$\mathbf{N}_u$ contains the hierarchical shape functions of the displacement field, $\mathbf{B}_u$ and $\mathbf{B}_p$ are the gradient matrices of the displacement and the capillary pressure field. The matrix $\mathbf{A}(\mathbf{n}_S)$ is the projection of ∇p_c on the crack channel characterized by the normal unit vector $\mathbf{n}_S$ of the crack surface $\partial_S\Omega$.

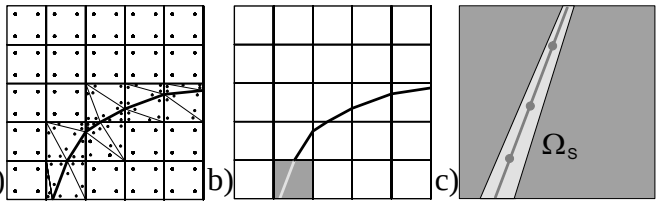

Figure 7: Integration concept: a) Integration of cracked and uncracked elements; b) Integration over the crack surface $\partial_S\Omega$; c) Integration along the crack channel Ω_S

The permeability matrix can be determined numerically as

$$\begin{aligned}\tilde{\mathbf{H}}_{pp} &= -\sum_{n=1}^{GP_p} \mathbf{B}_p^T\, \mathbf{k}_f/\mu_l\, \mathbf{B}_p |\mathbf{J}_n| \alpha_n \\ &\quad - \sum_{j=1}^{GP_c} \mathbf{B}_p^T\, \mathbf{A}^T\, k_c^t(w)/\mu_l\, \mathbf{A}\, \mathbf{B}_p\, w_j\, |\mathbf{J}_{\partial_S\Omega,j}|\, \alpha_j\end{aligned} \tag{32}$$

using GP_p integration points for the continuum and GP_c integration points for the crack channel (see Figure 7). The crack width w_j and the Jacobian determinant of the crack surface $|\mathbf{J}_{\partial_S\Omega,j}|$ are evaluated at the integration point j with the corresponding weight factor α_j. The integration is performed either over triangles or quadrilaterals representing the midsurfaces of the crack channel in anology to the integration of the traction-separation law for cohesive cracks.

7 NUMERICAL EXAMPLE

The applicability of the proposed finite element formulation for concrete structures considering moisture transport in cracks is demonstrated by means of hygro-mechanical analyses of a cracked beam subjected first to external loading. The material and geometry parameters are chosen as follows: Young's modulus $E = 2000\,[N/mm^2]$, Poisson's ratio $\nu = 0.2\,[N/mm^2]$, thickness $t = 10\,[mm]$ and liquid permeability $k_0 = 2.77 \cdot 10^{-21}\,[m^2]$.

Figure 8 contains the geometry, the mechanical and hygral boundary conditions and the spatial discretization with 272 3D-p-elements. For the approximation of the regular displacement field, a polynomial degree $p = 2$ is choosen in the plane of the structure and $p = 1$ in thickness direction, whereas trilinear shape functions are used for the enhanced displacement field and for the capillary pressure field.

The diagram in Figure 9 illustrates the mechanical and hygral loading history of the beam structure. After applying a displacement $u^* = 0.56\,mm$ on the top of the beam, a drying process at the lower boundary Γ^2 from a liquid saturation of $S_l^{*2} = 88.2\,\%$ ($p_c = 10.0\,N/mm^2$) to a final saturation of $S_l^{*2} = 58.8\,\%$ ($p_c = 20.0\,N/mm^2$) is prescribed, while the liquid saturation S_l^{*1} at the upper boundary Γ^1 remains constant. As a consequence of the external loading a crack of $3.25\,mm$ at the bottom side along the centerline of the beam develops. Due to the drying process, a further crack opening is observed (Figure 10).

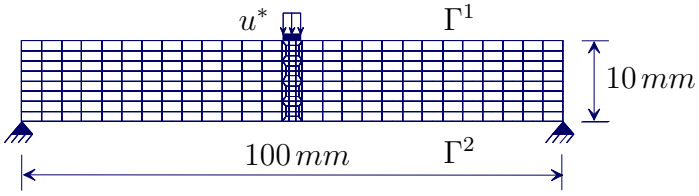

Figure 8: Numerical Example: System and Loading

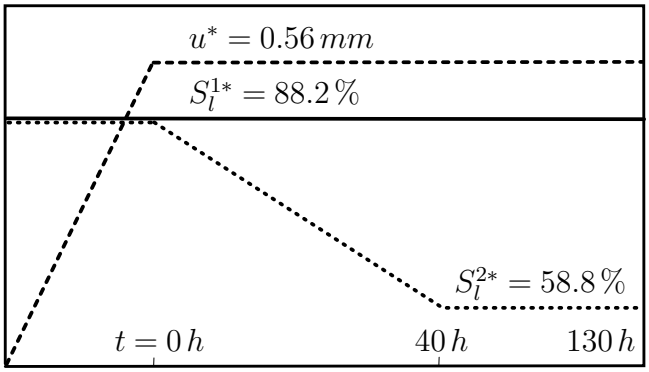

Figure 9: Numerical Example: Mechanical and hygral loading history

The capillary pressure distribution shown in Figure 11 illustrates the effect of the accelerated moisture transport through the crack on the moisture distribution after 40, 70, 100 and 130 hours. According to the prescribed hygral boundary conditions, the drying front penetrates the beam starting from the bottom face. In the vicinity of the crack, an increasing pore pressure corresponding to an accelerated drying process is observed.

8 CONCLUSIONS

In this paper a three-dimensional finite element discretization concept for hygro-mechanically analyses

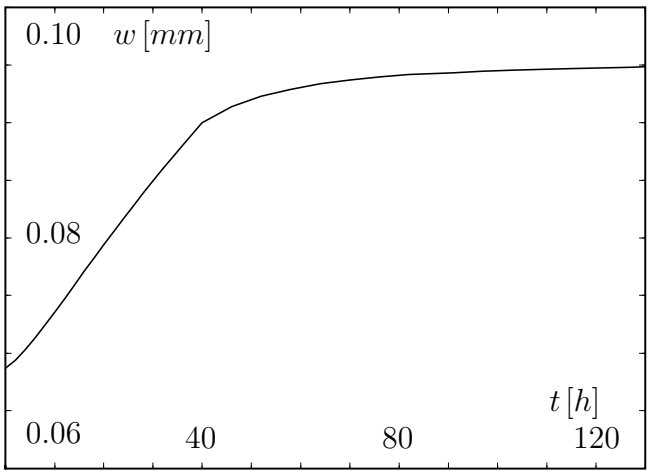

Figure 10: Numerical Example: Evolution of crack opening during drying

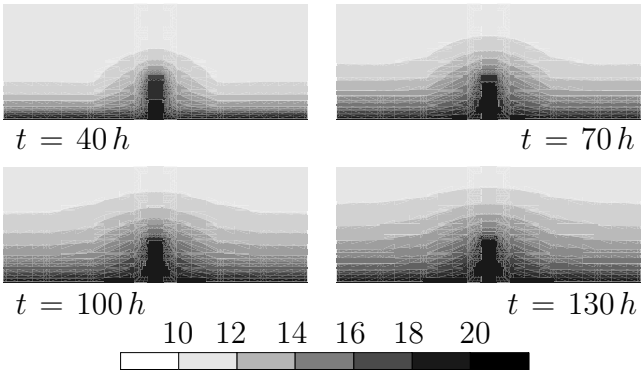

Figure 11: Numerical Example: Pore Pressure Distribution $p_c\,[N/mm^2]$

of partially saturated concrete structures considering cracks has been presented. It is characterized by using the Extended Finite Element Method (X-FEM) in conjunction with a p-finite element based on a hierarchical formulation of higher order shape functions and a hygro-mechanical model for partial saturated materials based upon the BIOT-COUSSY theory for the uncracked material. Moisture transport in the crack channel has been taken into account considering the topology of the crack channel. Details of the finite element formulation and of the threedimensional numerical integration using different subdomains for the continuum part and the crack are provided in the paper. As far as the moisture flux orthogonal to the crack is concerned, the discrete character of the crack is not yet fully considered in the present formulation. This will be taken into account in an enhanced version of the model currently in progress. The applicability of the model has been demonstrated by means of a 3D benchmark example.

9 ACKNOWLEDGMENT

Financial support was provided by the German National Science Foundation (DFG) in the framework of the project B3 of the collaborative research center SFB 398. This support is gratefully acknowledged.

REFERENCES

Abellan, M., R. de Borst, and J. Bergheau (2005). Analysis of discontinuities in fluid-saturated porous media. In A. Carpinteri (Ed.), *International Conference on Fracture (ICF 11)*.

Aldea, C.-M., M. Ghandehari, S. Shah, and A. Karr (2000). Estimation of water flow through cracked concrete under load. *ACI Materials Journal 97*, 567–575.

Ander, M. and A. Samuelsson (2001). Geometrically nonlinear analysis of thin shells by use of p-hierarchical solid elements. In *European Conference on Computational Mechanics*, Cracow, Poland. CD-Rom.

Areias, P. and T. Belytschko (2005). Analysis of threedimensional crack initiation and propagation using the extended finite element method. *International Journal for Numerical Methods in Engineering 63*, 760–788.

Baroghel-Bouny, V., M. Mainguy, T. Lassabatère, and O. Coussy (1999). Characterization and identification of equilibrium and transfer moisture properties for ordinary and high-performance cementitious materials. *Cement and Concrete Research 29*, 1225–1238.

Barton, N., S. Bandis, and K. Bakhtar (1985). Strength, deformation and conductivity coupling of rock joints. *International Journal of Rock Mechanics and Mining Sciences & Geomechanics Abstracts 22*, 121–140.

Bear, J. and Y. Bachmat (1991). *Introduction to Modeling of Transport Phenomena in Porous Media*. Dordrecht, The Netherlands: Kluwer Academic Publisher.

Becker, C., D. Kuhl, and G. Meschke (2005, June). Higher order discretization concepts for multifield durability analysis. In E. Ramm, W. Wall, K.-U. Bletzinger, and M. Bischoff (Eds.), *Online Proceedings of the 5^{th} International Conference on Computation of Shell and Spatial Structures*, Salzburg, Austria. www.iassiacm2005.de.

Becker, C. and G. Meschke (2004). A higher order 3D multifield finite element formulation for durability analyses of structures. In F. Stangenberg, O. T. Bruhns, D. Hartmann, and G. Meschke (Eds.), *2nd International Conference Lifetime Oriented Design Concepts*, Bochum, Germany, pp. 309–318.

Coussy, O. (2004). *Poromechanics*. Chichester, England: Wiley.

Coussy, O. and F.-J. Ulm (2001). Elements of durability mechanics of concrete structures. In Z. B. F.-J. Ulm and F. Wittmann (Eds.), *Creep, Shrinkage and Durability Mechanics of Concrete and Other Quasi-Brittle Materials*, Oxford, pp. 393–409. Elsevier.

Düster, A. (2002). *High order finite elements for threedimensional, thin-walled nonlinear continua*. Aachen: Shaker Verlag. Dissertation, Technische Universität München.

Düster, A., A. Niggl, and E. Rank (2002). Thermoelastic computations of geomatrically non-linear threedimensional thin-walled continua based on high order finite elements. In H. Mang, F. Rammerstorfer, and J. Eberhardsteiner (Eds.), *Fifth World Congress on Computational Mechanics*, Vienna, Austria.

Düster, A. and E. Rank (2002). A p-version finite element approach for two- and three-dimensional problems of the J2 fbw theory with non-linear isotropic hardening. *International Journal for Numerical Methods in Engineering 53*, 49–63.

Ehlers, W. and P. Ellsiepen (2001). Theoretical and numerical methods in environmental continuum mechanics based on the Theory of Porous Media. In B. Schrefler (Ed.), *Environmental Geomechanics*, Volume 417 of *CISM Courses and Lectures*, Wien, Austria, pp. 1–81. Springer-Verlag.

Gasser, T. and G. Holzapfel (2005). Modeling 3D crack propagation in unreinforced concrete using PUFEM. *Computer Methods in Applied Mechanics and Engineering 194*, 2859–2896.

Grasberger, S. and G. Meschke (2003). Drying shrinkage, creep and cracking of concrete: From coupled material modelling to multifield structural analyses. In R. DeBorst, H. Mang, N. Bićanić, and G. Meschke (Eds.), *Computational Modelling of Concrete Structures*, pp. 433–442. Balkema.

Gravouil, A., N. Moës, and T. Belytschko (2002). Non-planar 3D crack growth by the extended finite element and level sets - Part II: Level set update. *International Journal for Numerical Methods in Engineering 53*, 2569–2586.

Jox, S., P. Dumstorff, and G. Meschke (2006). Aspects of crack propagation and hygro-mechanical coupling using X-FEM. In *III European Conf. on Computational Mechanics (ECCM)*. Springer Verlag.

Kuhl, D., F. Bangert, and G. Meschke (2004). Coupled chemo-mechanical deterioration of cementitious materials. Part II: Numerical methods and simulations. *International Journal of Solids and Structures 41*, 41–67.

Lewis, R. and B. Schrefler (1998). *The FInite Element Method in the Static and Dynamic Deformation and Consolidation of Porous Media*. Chichester: John Wiley & Sons.

Meschke, G. and S. Grasberger (2003). Numerical modelling of coupled hygro-mechanical degradation of cementitious materials. *Journal of Enggineering Mechanics(ASCE) 129*, 383–392.

Moës, N., J. Dolbow, and T. Belytschko (1999). A finite element method for crack growth without remeshing. *International Journal for Numerical Methods in Engineering 46*, 131–150.

Moës, N., A. Gravouil, and T. Belytschko (2002). Non-planar 3D crack growth by the extended finite element and level sets - Part I: Mechanical model. *International Journal for Numerical Methods in Engineering 53*, 2549–2568.

Mualem, Y. (1976). A new model for predicting the hydraulic conductivity of unsaturated porous media. *Water Resources Research 12*, 513–522.

Osher, S. and R. Fedkiw (2003). *Level Set Methods and Dynamics Implicit Surfaces*. New York: Springer.

Oshita, H. and T. Tanabe (2000). Water migration phenomenon model in cracked concrete. II: Calibration. *Journal of Engineering Mechanics (ASCE) 126*, 544–549.

Snow, D. (1969). Anisotropic permeability of fractured media. *Water Resources Research 5*, 1273–1289.

Sukumar, N., D. Chopp, and B. Moran (2003). Extended finite element method and fast marching method for three-dimensional fatigue crack propagation. *Engineering Fracture Mechanics 70*, 29–48.

Sukumar, N., N. Moës, B. Moran, and T. Belytschko (2000). Extended finite element method for three-dimensional crack modelling. *International Journal for Numerical Methods in Engineering 48*, 1549–1570.

Szabó, B., A. Düster, and E. Rank (2004). *Encyclopedia of Computational Mechanics*, Chapter The p-version of the finite element method. John Wiley and Sons.

van Genuchten, M. (1980). A closed-form equation for predicting the hydraulic conductivity of unsaturated soils. *Soil Science Society of America 44*, 892–898.

Wells, G. and L. Sluys (2001). Three-dimensional embedded discontinuity model for brittle fracture. *International Journal of Solids and Structures 38*, 897–913.